# Advanced Characterization Approaches with Pad-Model De-Embedding of sub-THz Devices for 6G Applications

Franzese, Aniello ; Sutbas, Batuhan; Mausolf, Thomas ; Moroni, Nicolò ; Negra, Renato ; Ramos, Alfredo Sánchez ; Greco, Francesco; Boccia, Luigi ; Shokrolahzade, Ehsan; Spirito, Marco

**DOI**
10.23919/EuMIC61603.2024.10732437

**Publication date**
2024

**Document Version**
Final published version

**Published in**
Proceedings of the 2024 19th European Microwave Integrated Circuits Conference (EuMIC)

# Advanced Characterization Approaches with Pad-Model De-Embedding of sub-THz Devices for 6G Applications

Aniello Franzese[12], Batuhan Sutbas[1], Thomas Mausolf[1], Nicolò Moroni[1], Renato Negra[2], Alfredo Sánchez Ramos[3], Francesco Greco[4], Luigi Boccia[4], Ehsan Shokrolahzade[5], Marco Spirito[5], Corrado Carta[16]

[1]IHP–Leibniz-Institut für innovative Mikroelektronik, Germany
[2]Chair of High Frequency Electronics, RWTH Aachen University, Germany
[3]Centro de Investigación y de Estudios Avanzados del IPN, Unidad Guadalajara, Mexico
[4]MAIC Laboratory, DIMES, Università della Calabria, Italy
[5]ELCA, TU Delft, The Netherlands
[6]Chair for Integrated Broadband and High Frequency Circuits, TU Berlin, Germany
franzese@ihp-microelectronics.com

***Abstract* — This work describes accurate methods for the characterization of sub-terahertz (sub-THz) devices and pad de-embedding procedures. The extraction of the intrinsic DUT is enabled by generating a precise pad model using two-tier calibration approaches. Moreover, the proposed approaches offer a solution to the designers to preserve precious silicon area by presenting a simplified and potentially parameterizable pad model. Employing two different thru-reflect-line (TRL) calibration kits (calKits) together with the DUT on the same die, this research validates the proposed calibration strategies. This paper uses as DUT at J-band, i.e. a Marchand balun, fabricated using IHP SiGe BiCMOS technology with an aluminum back-end-of-line (BEOL), alongside the mentioned calKits. The goal of the paper is to assess the performance of the DUT and validate two de-embedding methods. Moreover, the pad model offers a way for accurate DUT characterization saving silicon area for future optimized designs.**

***Keywords* — 6G, balun, characterization, J-band, sub-THz, TRL.**

## I. Introduction

Following the introduction of the IEEE 802.15.3d standard, the bandwidth (BW) spanning 252 GHz to 325 GHz is set to enable high data rates for the sixth-generation of wireless communications (6G) and beyond [1]. The high BW enables the design of integrated circuits which accommodate high frequency signals with unprecedented data rates, potentially exceeding 100 Gbit/s. Such systems supporting high data rates pave the way to a multitude of unforeseen applications such as autonomous cars, joint communication and sensing, robotic medicine, new applications in data centers, and 6G back-haul.

Numerous excellent studies have already proposed advancements at the subterahertz (sub-THz) frequencies for various building blocks, including low-noise amplifiers (LNAs) [2], frequency multipliers [3], power amplifiers (PAs) [4], and full transceivers [5] as well. These works operating in the sub-THz region is known for the complicated measurement procedure when interfacing circuits with probes and vector network analyzers (VNAs). Therefore, a precise characterization becomes imperative. While commercial calibration kits (calKits) offer thru-reflect-line (TRL) structures, whose use have been widely adopted as a reliable method, setting the reference plane at the probe tips and transferring the cal to a different substrate (i.e. moving from alumina to silicon) has been shown to reduce the calibration quality [6]. To address this issue, the authors have developed two on-wafer calKits following the approaches presented in [7], [8]. A first 30-Ω calKit is used for the 1st-tier calibration to move the reference plane to the probe tips and get the response of the DUT including the pads, whereas a second 50-Ω calKit serves two separate roles: primarily to extract the behaviour of the pads (using the 1st-tier calibration achieved with the 30-Ω calKit) and deriving their model, and secondarily to obtain the intrinsic DUT measurement (this time, employing a new calibration with the latter calKit). After the pad model has been extracted, its behaviour can be de-embedded [9]. Moreover, the obtained model can then be reused to de-embed future designs, when the pad interface is kept. The circuit designer does not need other de-embedding structures, having already a response provided by this simple model, which could be parameterized. Thereby, saving further silicon area. Finally, a J-band Marchand balun is designed and employed as DUT, validating the proposed approaches.

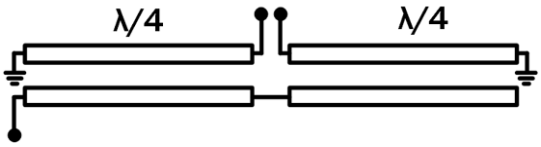


Fig. 1. Schematic of a conventional Marchand balun used as DUT

## II. Design of the Marchand Balun

One of the most common balun topology used as a reliable on-chip interface between the differential circuits

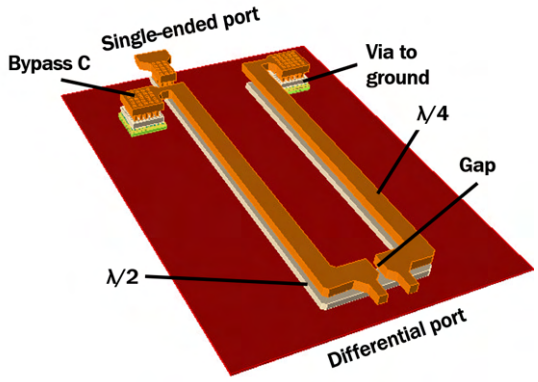


Fig. 2. Three-dimensional view of the sub-THz J-band Marchand balun

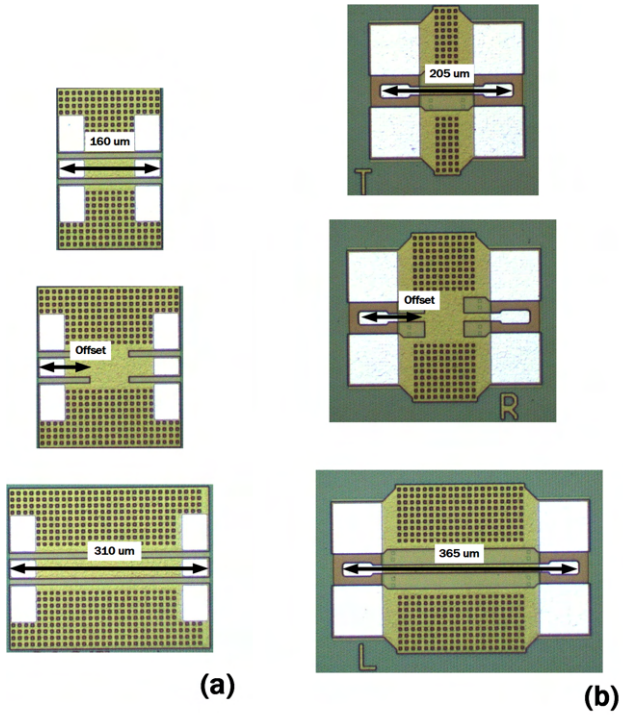


Fig. 3. Micrograph of the fabricated thru (top), reflect (middle), and line (bottom) standards for (a) 30-Ω, and (b) 50-Ω calKits.

and the single-ended probes at frequencies above 100 GHz is the Marchand balun. The schematic of a conventional balun is shown in Fig. 1. This configuration has been largely analysed in [10], [11] and is mostly based on transmission lines (TLs) [12]. Therefore, the proposed design utilizes broadside-coupled TLs, tackling impairments encountered in the sub-THz region [13], [14]. Nevertheless, the Marchand balun can achieve perfect amplitude and phase difference with a negligible separation between its differential ports, as shown in Fig. 2. However, a practical design necessitates connecting the differential ports to TLs, which introduces a gap. Consequently, the single-ended termination is exposed to a TL which becomes marginally longer then $\lambda/2$. This adjustment is due to the length of the two $\lambda/4$ TLs and the


Fig. 4. Pad model using (a) T-shaped impedance equivalent and (b) lumped elements

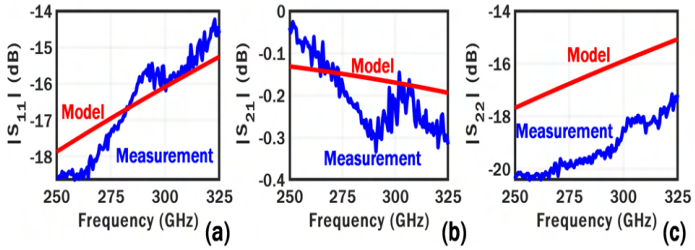


Fig. 5. Measured and modeled $S$-parameters of the pad: (a) $|S_{11}|$, (b) $|S_{21}|$, and (c) $|S_{22}|$ against the frequency.

gap on the differential side, degrading the performance of the balun. Nevertheless, the additional line segment can be fine-tuned by electromagnetic (EM) simulations [13]. Another pitfall at sub-THz frequencies are the imperfections given by the nonideal ground. In a conventional design, the two $\lambda/4$ TLs belonging to the differential ports must be connect to ground often through vias. In EM simulations, the vias are typically oversimplified, leading to discrepancies between simulations and actual measurements. To address this issue, two bypass capacitors are placed at the very end of the $\lambda/4$ TLs, serving as RF ground. Measurements along with the de-embedding of the pads are then required to validate the behaviour of the intrinsic J-band Marchand balun.

## III. Calibration Kits

As mentioned before, two different calKits have been designed both for TRL calibration, each serving a distinct purpose. The first calKit is based on homogeneous 30-Ω TLs, and it is used as 1$^{st}$-tier calibration, more specifically it sets the VNA response and reference plane, i.e. center of the thru. Moreover, employing homogeneous TLs allows to easily move (back) the reference plane to the probe tips by using the propagation constant, $\gamma$, of the TL extracted during the calibration. The necessity of such a calKit is mostly practical. Indeed, the low-impedance TL offers a line width which does not need the use of pads, removing the errors associated to the width discontinuities of the pad-to-line transition [8]. The 30-Ω calKit, shown in Fig. 3a, comprises three standards: the thru, the reflect, and the line. Similarly, the 50-Ω one, depicted in Fig. 3b has the same structures. However, there is a difference in the TL widths between these two calKits. Specifically, the TL width in the 50-Ω calKit is narrower than that of the 30-Ω one. This reduction in width necessitates the use of pads to ensure proper landing of the probes. The application of the 50-Ω calKit is twofold. Firstly, it facilitates the extraction of the pad response, after calibrating the 30-Ω kit. Secondly, it

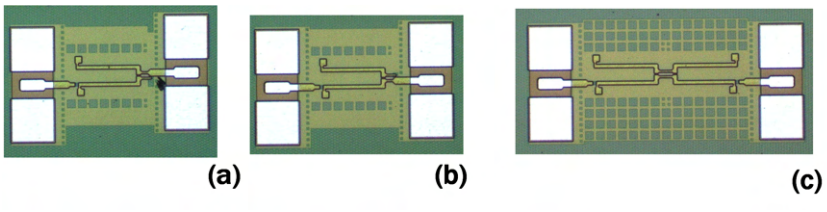


Fig. 6. Micrographs of the fabricated Marchand balun test structures in (a) single-ended to single-ended in-phase, (b) single-ended to single-ended out-of-phase, and (c) back-to-back configuration.

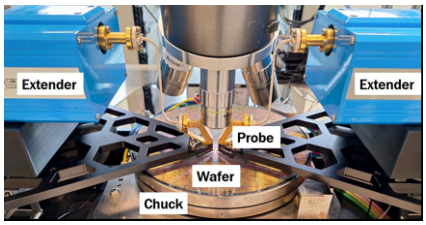


Fig. 7. Measurement setup used to probe the 8-inch wafer

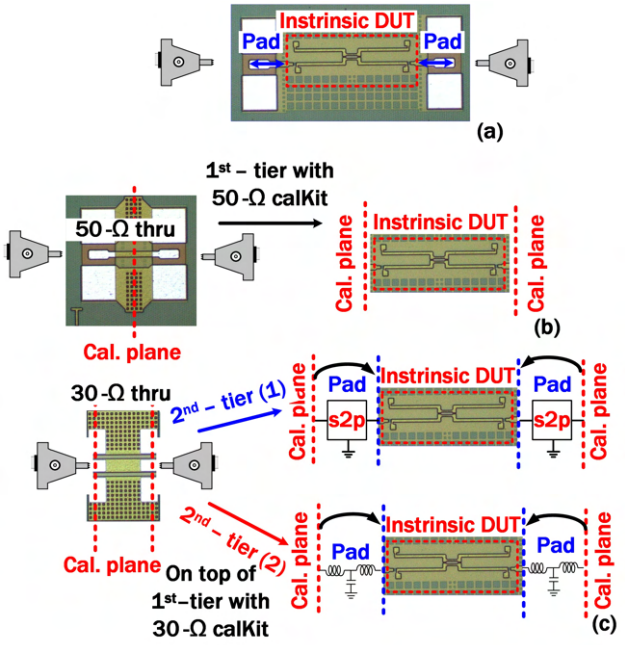


Fig. 8. Measurement procedure of the DUT: (a) raw-data acquisition, (b) applying 1st-tier calibration with the 50-Ω calKit, and (c) applying 2nd-tier on top of a calibration with 30-Ω calKit, using $S$-parameters of the pad and its lumped-component model.

enables the determination of the intrinsic behaviour of the DUT. This measurement can then be validated by comparing it with the results obtained after de-embedding the pad model from the initial calibration, namely 1st-tier using the 30-Ω calKit. Through this double approach the accuracy of the calibration process is not only validated, but also the detailed response of the intrinsic DUT can be extracted. Moreover, the pad model can be parameterized and reused by the designer without the need of using further silicon area.

## IV. Pad Modeling

The pad model is of paramount relevance in the design procedure. Having precise knowledge of the parasitics is necessary to evaluate the DUT performance. In designing the model, one can extract the pad behaviour can be extracted from $S$-parameter measurements, converting them into admittance or impedance parameters. A $\pi$-circuit is typically used with admittance parameters, whereas a T-shaped equivalent circuit is employed for impedance parameters, which can be easily calculated. Then, $S$-parameters of the extracted pad behaviour can be easily transformed into a $Z$-matrix, and $Z_A$, $Z_B$, and $Z_C$ of the T-shaped circuit, shown in Fig. 4a, can be written as

$$Z_A = Z_{11} - Z_{12}, \tag{1}$$
$$Z_B = Z_{22} - Z_{12}, \tag{2}$$
$$Z_C = Z_{12} \tag{3}$$

where $Z_{11}$, $Z_{12}$, and $Z_{22}$ are related to the $Z$-matrix. In Fig. 4b, $Z_A$ is modeled as $R_A$ and $L_A$, $Z_B$ can be seen as the series combination of $R_B$ and $L_B$, whereas $Z_C$ can be given by $R_C$ and $C_C$. These parameters could then be used to create a parameterized cell with opportune evaluations. The values extracted from the measurements are $L_A = 17.2\,\text{pH}$, $L_B = 4.22\,\text{pH}$, and $C_C = 6.13\,\text{fF}$. Nevertheless, only $R_A = 0.66\,\Omega$ has a physical meaning, since the other two resistive elements are negligible or negative.

## V. Measurement Results

Three test structures have been fabricated for this study, as shown in Fig. 6. The first two structures facilitate the characterization of single-ended to single-ended phase difference between in-phase (see Fig. 6a) and out-of-phase (see Fig. 6b) ports. Conversely, the third structure, presented in Fig. 6c, comprises a back-to-back configuration used to validate the loss. The Marchand balun utilizes the two top thick metals of the back-end-of-line (BEOL) for its TLs and has a size of $145\times75\,\mu\text{m}^2$. The measurement setup is presented in Fig. 7, where an 8-inch wafer is installed on a metal chuck and probed with WR3-waveguide probes. The probes land on the DUT pads to acquire the raw data as shown in Fig. 8a. Three different calibration methods have been used. The first, namely 1st-tier, is performed using the 50-Ω calKit moving the reference plane at the center of the thru, as per Fig. 8b. Therefore, with this calibration the measurement of the DUT provides a direct de-embedding of the pads.

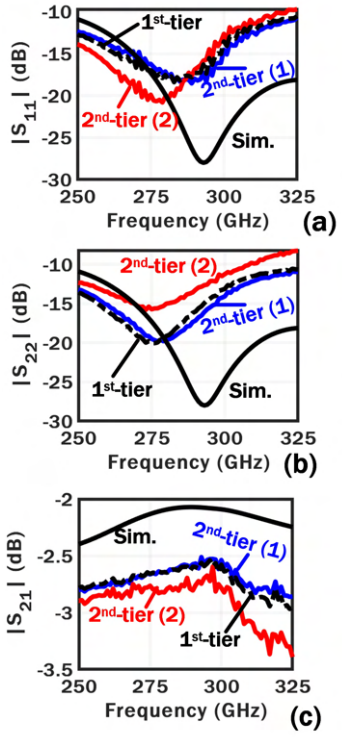


Fig. 9. Intrinsic back-to-back measured and simulated $S$-parameters of the balun: (a) $|S_{11}|$, (b) $|S_{22}|$, and (c) $|S_{21}|$ against frequency, using the mentioned pad de-embedding techniques.

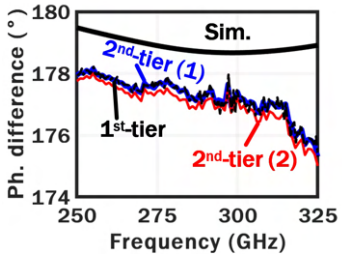


Fig. 10. Measured and simulated phase difference of the two single-ended-to-single-ended balun structures against the frequency, de-embedding the pad behaviour.

The 2nd-tier calibration is achieved on top of the calibration performed using the 30-Ω calKit and then de-embedding the pads, as reported in Fig. 8c. the 2nd-tier (1) calibration isolates the DUT de-embedding the pad behaviour through previous measurements, whereas 2nd-tier (2) utilizes the pad model given in the previous section.

Measured $S$-parameters are shown in Fig. 9, where 1st-tier and 2nd-tier (1) are overlapping each other. Even though 2nd-tier (2) follows closely the trend of the previous methods, $S_{11}$ in Fig. 9a and $S_{22}$ in Fig. 9b show a shift in frequency. This should be taken into account when designing the circuit, whereas for the phase difference the three methods do not show tangible discrepancies as reported in Fig. 10. Finally, the methods presented demonstrate optimal agreement with simulation results, showing an offset of approximately 0.6 dB and a phase difference with maximum offset of 4°.

## VI. Conclusion

This paper presents different approaches in the characterization of DUT for sub-THz applications. Through the fabrication of custom 30-Ω and 50-Ω on-wafer calKits and the introduction of a pad model, this study provides accurate $S$-parameter measurements and pad de-embedding procedures. The three different approaches validate the measurements and the close alignment with simulation results underlines their precision and reliability.

## Acknowledgment

The authors thank the Technology Department of IHP GmbH for the chip manufacturing and the Earl McCune/XG Labs, TU Delft for the help with the measurements.

## References

[1] "IEEE standard for high data rate wireless multi-media networks–amendment 2: 100 Gb/s wireless switched point-to-point physical layer," *IEEE Std*, pp. 1–55, 2017.

[2] A. Gadallah, M. H. Eissa, T. Mausolf, D. Kissinger, and A. Malignaggi, "A 300-GHz low-noise amplifier in 130-nm SiGe SG13G3 technology," *IEEE Microwave and Wireless Components Letters*, vol. 32, no. 4, pp. 331–334, 2022.

[3] A. Ali, J. Yun, M. Kucharski, H. J. Ng, D. Kissinger, and P. Colantonio, "220–360-GHz broadband frequency multiplier chains (x8) in 130-nm BiCMOS technology," *IEEE Transactions on Microwave Theory and Techniques*, vol. 68, no. 7, pp. 2701–2715, 2020.

[4] M. H. Eissa, G. Fischer, T. Mausolf, H. Rücker, A. Malignaggi, and G. Kahmen, "220–320-GHz J-band 4-way power amplifier in advanced 130-nm BiCMOS technology," *IEEE Microwave and Wireless Components Letters*, vol. 32, no. 11, pp. 1335–1338, 2022.

[5] I. Abdo, T. Fujimura, T. Miura, *et al.*, "A 300 GHz wireless transceiver in 65 nm CMOS for IEEE802.15.3d using push-push subharmonic mixer," in *2020 IEEE/MTT-S International Microwave Symposium (IMS)*, 2020, pp. 623–626.

[6] L Galatro and M Spirito, "Analysis of residual errors due to calibration transfer in on-wafer measurements at mm-wave frequencies," in *2015 IEEE Bipolar/BiCMOS Circuits and Technology Meeting-BCTM*, IEEE, 2015, pp. 141–144.

[7] D. F. Williams, A. C. Young, and M. Urteaga, "A prescription for sub-millimeter-wave transistor characterization," *IEEE Transactions on Terahertz Science and Technology*, vol. 3, no. 4, pp. 433–439, 2013.

[8] L. Galatro, A. Pawlak, M. Schroter, and M. Spirito, "Capacitively loaded inverted CPWs for distributed TRL-based de-embedding at (sub) mm-waves," *IEEE Transactions on Microwave Theory and Techniques*, vol. 65, no. 12, pp. 4914–4924, 2017.

[9] L. Galatro and M. Spirito, "Millimeter-wave on-wafer TRL calibration employing 3-D EM simulation-based characteristic impedance extraction," *IEEE Transactions on Microwave Theory and Techniques*, vol. 65, no. 4, pp. 1315–1323, 2017.

[10] C.-H. Lien, C.-H. Wang, C.-S. Lin, P.-S. Wu, K.-Y. Lin, and H. Wang, "Analysis and design of reduced-size marchand rat-race hybrid for millimeter-wave compact balanced mixers in 130-nm CMOS process," *IEEE transactions on microwave theory and techniques*, vol. 57, no. 8, pp. 1966–1977, 2009.

[11] H. Ghaleb, D. Fritsche, C. Carta, and F. Ellinger, "Design and characterization of a 180-GHz on-chip integrated broadband balun," in *2018 IEEE Radio and Wireless Symposium (RWS)*, 2018, pp. 237–239.

[12] A. Ali, J. Yun, H. Jalli Ng, D. Kissinger, F. Giannini, and P. Colantonio, "High performance asymmetric coupled line balun at sub-THz frequency," *Applied Sciences*, vol. 9, no. 9, p. 1907, 2019.

[13] C.-H. Lin, C.-H. Wu, G.-T. Zhou, and T.-G. Ma, "General compensation method for a marchand balun with an arbitrary connecting segment between the balance ports," *IEEE Transactions on Microwave Theory and Techniques*, vol. 61, no. 8, pp. 2821–2830, 2013.

[14] P. Stärke, C. Carta, and F. Ellinger, "A deembedding method for reciprocal three-port devices demonstrated with 200-GHz baluns," *IEEE Microwave and Wireless Components Letters*, vol. 29, no. 1, pp. 11–13, 2019.